Papers

Volume 7: 2004-2008

Thoft-Christensen, Palle

Publication date:
2008

Document Version
Publisher's PDF, also known as Version of record

CHAPTER 136

NUMERICAL STUDY OF CORROSION CRACK OPENING[1]

P. Thoft-Christensen, H.L. Frandsen & S. Svensson
Aalborg University, Aalborg, Denmark

ABSTRACT

Determining the reliability of reinforced concrete structures, based on visual inspection of corroding cracks on the surfaces of structures, is of great interest. In the present study, models for the deterioration of reinforced concrete structures are presented with special emphasis on a model for the corrosion crack opening. Experiments and theoretical analysis by a numerical final element method (FEM), support that the reduction of the reinforcement bar diameter due to corrosion is proportional to the corresponding increase in crack width, measured on the surface of a concrete specimen, for a given time interval.

More recently, the constant of proportionality, the so-called crack-corrosion index, has been studied further with respect to its dependence on the diameter of the reinforcement and the concrete cover. In the present paper, the above work is presented and extended with more realistic 3D-models of the cracked concrete beam. The crack-corrosion index is evaluated for variations of different parameters, such as bar diameter, concrete cover, crack length, and type of corrosion product. This paper is an extended version of a paper by Thoft-Christensen et al. [1] presented at the IFIP WG 7.5 Conference, Aalborg, Denmark, May 2005.

1. INTRODUCTION

Life-cycle assessment of the structural reliability of a reinforced concrete structure is based on models for the deterioration of concrete and corrosion of reinforcement. The most serious effect of deterioration on the load carrying capacity is corrosion of the reinforcement. Chloride penetration of the concrete presents a hostile environment and is considered the most common reason for corrosion of reinforcement. Models for the

[1] Accepted for publication in "Structure and Infrastructure Engineering", 2008.

corrosion initiation are, therefore, often based on Fick's law for diffusion of chloride in concrete; see e.g. Thoft-Christensen [2]. After initiation of corrosion in the reinforcement, the cross-section of the reinforcement is frequently assumed to decrease with time. With the models it is simple to perform a deterministic or stochastic estimate of the so-called reliability profile, i.e. the capacity or the reliability as functions of time; see e.g. Thoft-Christensen [3]. The reliability profile consists of six parts:

1. Chloride penetration,
2. Corrosion initiation,
3. Corrosion evolution,
4. Initial cracking,
5. Crack propagation,and
6. Spalling.

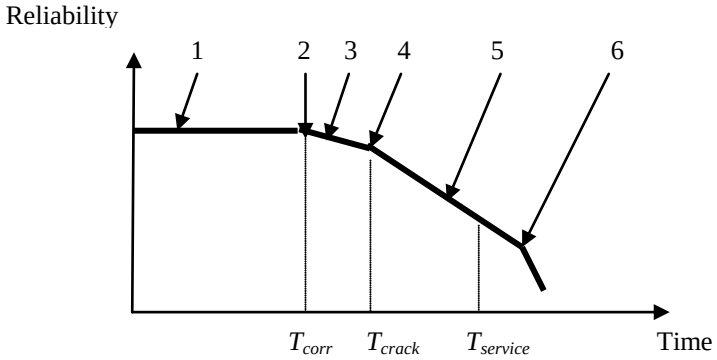

Figure 1. Deterioration steps where T_{corr}, T_{crack} and $T_{service}$ are time to initiation of corrosion, time to initiation of crack and service life of structure, respectively.

Deterioration steps 1-4 are well understood, and are presented in numerous papers; see e.g. Liu and Weyers [4]. A deterministic approach based on FEM analysis is used by e.g. Du et al. [5] and Bhargava et al. [6], and a stochastic approach based on Monte-Carlo simulation is used by e.g. Thoft-Christensen [7] and Thoft-Christensen [8], for example. Steps 5 and 6 have only recently been investigated by Thoft-Christensen [3].

Applying diffusion models to estimate chloride penetration of concrete shows that, for a considered example, the time to initiation of corrosion can be described with a Weibull distribution. This approach, based on diffusion theory, seems to have reached general acceptance among researchers in this field. The time to crack initiation is determined from the volume of corrosion products and the required space to facilitate this volume in the concrete. Initially, the rust products will fill the interconnected porous zone completely and then result in an expansion of the concrete near the reinforcement. As a result of this, tensile stresses are initiated in the concrete. With continued corrosion, the tensile stresses will reach a critical value and corrosion cracks will develop. For reinforcement relatively close to the concrete surface, the developed cracks will be visible. After formation of the initial crack, the rebar cross-section is further reduced due to the continued corrosion, and the width of the crack increases. As discussed and applied in the following sections, experiments show that the reduction of the rebar diameter ΔD_{bar} is proportional to the corresponding increase in crack width opening Δw_{crack}, measured on the surface of the concrete specimen, i.e. $\Delta w_{crack} \propto \Delta D_{bar}$.

2. CRACK-CORROSION INDEX

Several researchers have investigated the evolution of corrosion cracks in reinforced concrete beams experimentally, e.g. Andrade et al. [9]. To reduce the duration of testing, artificial corrosion by electrical current is a common experimental approach. During the test, the loss of rebar cross-section is monitored and the corresponding crack evolution is measured by strain gauges attached to the surface of the specimen. In the study by Andrade et al. [9], four simple test specimens were investigated. The specimens were small reinforced concrete beams with only a single rebar with a 20 or 30 mm concrete cover. In figure 2, the results from this experimental study are shown.

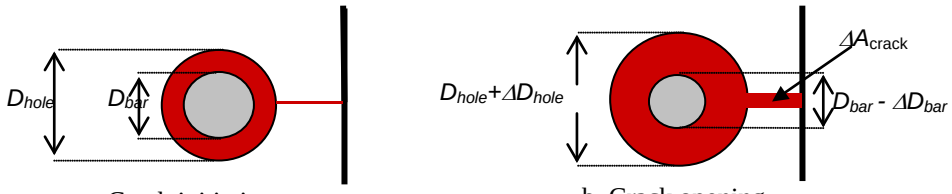

a. Crack initiation b. Crack opening

Figure 3. Schematic illustration of the notation displayed on the crack shown at two different stages of the cracking.

Table 1. Values of α for different corrosion products, Nielsen [10].

Corrosion product	Colour	α
Fe_3O_4	Black	2.1
$Fe(OH)_2$	White	3.8
$Fe(OH)_3$	Brown	4.2
$Fe(OH)_3$, $3H_2$	Yellow	6.4

The total increase of the volume per length due to cracking, ΔA_{exp}, results from reduction of bar diameter ΔD_{bar}, expansion of the hole diameter ΔD_{hole}, and increased crack opening ΔA_{crack} and may be written as

$$\Delta A_{exp} = \frac{\pi}{2}\Delta D_{bar} D_{bar} + \frac{\pi}{2}\Delta D_{hole} D_{hole} + \Delta A_{crack} \tag{3}$$

With the additional assumption that at crack initiation $D_{bar} \approx D_{hole}$, the cross sectional areas found in equations (2) and (3) ΔA_{rust} ΔA_{exp} are identical, and the relation between reduction of steel bar diameter and expansion of hole diameter becomes

$$(\alpha - 1)\Delta D_{bar} \approx \Delta D_{hole} + \frac{2\Delta A_{crack}}{\pi D_{hole}} \tag{4}$$

and, from the definition of the crack corrosion index

$$\gamma = \frac{\Delta w_{crack}}{\Delta D_{bar}} \approx (\alpha - 1)\frac{\Delta w_{crack}}{\Delta D_{hole} + 2\Delta A_{crack} / \pi D_{hole}} \tag{5}$$

To estimate the shape changes of crack, a series of 2D and 3D FEM-simulations have been performed. The results of these are presented in the sections 3 and 4 respectively.

3. 2D-MODELLING OF THE EXPANDING CRACK IN A BEAM CROSS-SECTION

The first simulations of the crack-corrosion index γ by a FEM analysis, was presented at the IFIP TC7 Conference on "System Modelling and Optimization" in Sophia Antipolis, France, July 2003, using the commercial FEM program FemLab; see Thoft-Christensen [11]. A rectangular beam cross-section with only one reinforcement bar was considered, see figure 4. The diameter of the hole around the rebar at the time of crack initiation was D_{hole} = 20 mm and the cover was c = 10 mm. The initial crack width was 0.01 mm.

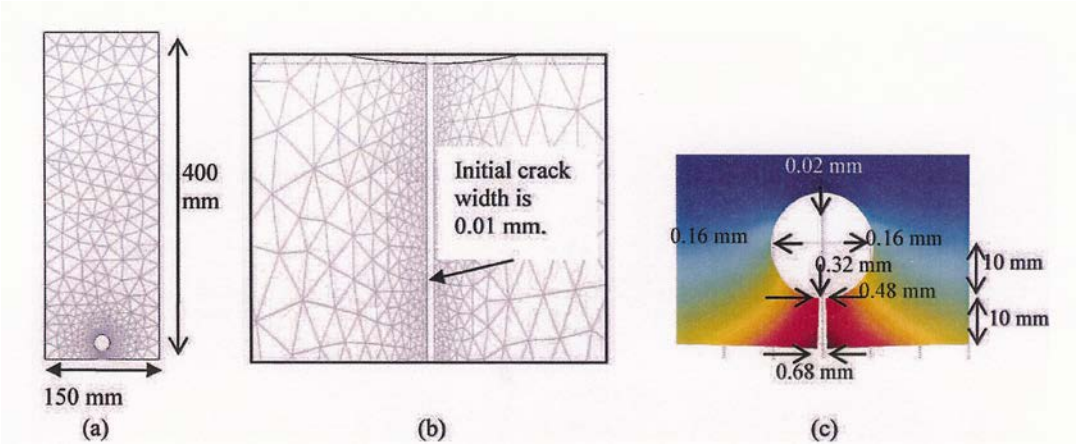

Figure 4. (a) the total FEM-mesh, (b) the local FEM-mesh in the vicinity of the crack, and (c) the calculated displacement field; Thoft-Christensen [11].

In the FEM model the rectangular cross-section in a long beam (plain strain) is assumed to have a centrally located reinforcement. A circular void, i.e. a hole, represents the reinforcement, and a initial crack with the width of 0.01 mm runs normal to the perimeter of the hole to the closest boundary of the concrete cross-section. The material is modelled as isotropic and linear elastic with a Young's modulus of $E = 25 \times 10^9$ Pa and Poisson's ratio of 0.2. Furthermore, the pressure caused by the expansion of corrosion products is represented by a uniform pressure normal to the perimeter of the hole. The magnitudes of pressure and Young's modulus are not important, since only the shape changes of the cross section in the elastic range are investigated.

Crack propagation can be modelled by an elasto-plastic constitutive law in combination with a suitable fracture criterion. These can be implemented in numerical methods such as X-FEM, or a meshless method. In stationary cracks, such as those studied here, no energy release from the cracking takes place. Furthermore, the high inelastic strains occur in a localised crack propagating zone at the crack ends and contribute very little to the deformations normal to the perimeter The deformations occurring in this stationary crack mat therefore be modelled by a linear elastic model to a good approximation.

For the example shown in figure 4, with a crack opening Δw_{crack} = 0.67 mm and an average increase of the hole diameter ΔD_{hole} = 0.31 mm the crack-corrosion index γ may be determined by equation (5) as

$$\gamma \approx (\alpha - 1)\frac{0.67}{0.31 + 2 \cdot 5.7/20\pi} = 1.36(\alpha - 1) \qquad (6)$$

or the crack-corrosion index is equal to 1.5 and 4.4 for black and brown rust, respectively; see table 1. This is in good agreement with the values obtained by the experiments by Andrade et al. [9] in section 2.

Table 2. Estimates of $\gamma(D_{bar},c)$.

Diameter D_{bar}, mm	Cover c, mm				
	20	25	30	35	40
10	3.72	3.53	3.39	3.30	3.25
12	3.93	3.76	3.63	3.55	3.50
14	4.09	3.94	3.83	3.75	3.71
16	4.20	4.08	3.99	3.92	3.88
18	4.26	4.19	4.11	4.06	4.03
20	4.28	4.27	4.21	4.18	4.15

The results of a similar FEM analysis of a cross-section similar to the one illustrated in figure 4 here, were presented for 10 different combinations of the cover c and the diameter D_{bar} in Thoft-Christensen [12]. The conclusion from that study, where the cover was smaller than the rebar diameter, is that γ increases

with the cover c for a fixed rebar diameter D_{bar}, and that γ also increased with the diameter D_{bar} for a fixed cover c.

A similar analysis with 30 combinations of D_{bar} and c, where the cover was larger than the rebar diameter, but with a different cross-section confirms this conclusion; see Thoft-Christensen [13]. The crack-corrosion indices γ for the 30 combinations are shown in table 2 for black rust. It is seen that γ for the analysed combinations increases with the diameter D_{bar} and decreases with the concrete cover c.

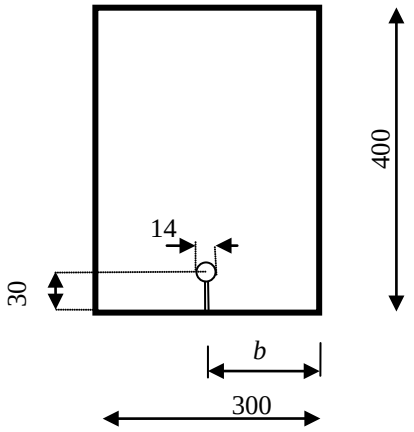

Figure 5. Cross-sectional dimensions with initial crack width of 0.01 mm (all dimensions in mm).

In the same paper the significance of the distance b from the crack to the nearest uncracked vertical side of the beam was important for the estimate of crack-corrosion index γ. The same cross-section was used, but the hole and the crack were placed at different distances b from the vertical side of the beam, see figure 5.

As an example of the results from this investigation by Thoft-Christensen [13], a rebar, with diameter D_{bar} = 14 mm and concrete cover c = 30 mm, and a variation of γ $\gamma(b) \approx \eta(b)$, where $\eta(b) = \Delta w_{crack} / \Delta D_{hole}$ for the distances b = 30, 60, 90, 120, and 150 mm is shown in figure 6. In this figure, $\eta(b)$ is shown as a function of b.

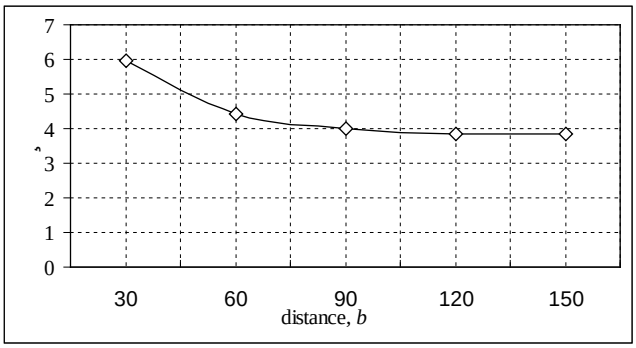

Figure 6. The function $\gamma(b) \approx \eta(b) = \Delta w_{crack} / \Delta D_{hole}$ for different distances, b , (mm) to the vertical edge.

The conclusion of this investigation is that the distance b to the vertical side of the beam is significant, if b is smaller than four times the rebar diameter. Otherwise, $\gamma(b) \approx \eta(b) = \Delta w_{crack} / \Delta, D_{hole}$ seems to be a good approximation.

4. 3D MODELLING OF AN EXPANDING CRACK

In this section, the procedure used in the 2D model of corrosion crack evolution is extended to a 3D model. The 2D model in section 3 is based on several assumptions, e.g. that the movement of corrosion products is restricted to the cross-section considered. In a 3D mode, the corrosion products may also move in the direction of the reinforcement. Furthermore, in a 3D model it is possible to consider situations where only parts of the reinforcement are corroded.

4.1 The FEM model

A beam element with the dimensions $400 \times 800 \times 1000$ mm is considered for the illustration of the FEM model. The size of the beam is of minor importance, as long as the influence of the boundary conditions can be neglected, as in the chosen setup. The model contains one centred rebar with the diameter D_{bar} and with a concrete cover c, see figure 7. Corrosion is positioned in the central part of the reinforcement with the length l ($0 < l < 1000$ mm). An initial crack connects the corroded part of the reinforcement with the surface of the beam as shown in figure 7. Corrosion is positioned in the central part of the reinforcement with a length l ($0 < l < 1000$ mm). An initial crack connects the corroded part of the reinforcement to the surface of the beam.

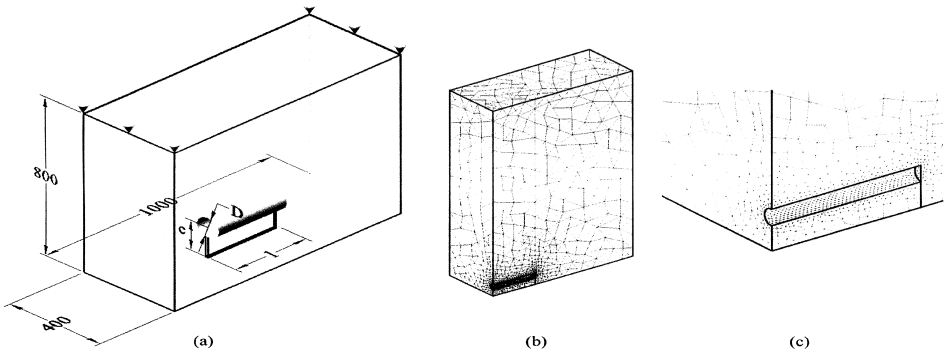

Figure 7. (a) The chosen boundary conditions for the FEM element model,
igure 7. (a) The chosen boundary conditions for the FEM element model,
gure 7. (a) The chosen boundary conditions for the FEM element model,
ure 7. (a) The chosen boundary conditions for the FEM element model,
re 7. (a) The chosen boundary conditions for the FEM element model,
e 7. (a) The chosen boundary conditions for the FEM element model,
 7. (a) The chosen boundary conditions for the FEM element model,
7. (a) The chosen boundary conditions for the FEM element model,
. (a) The chosen boundary conditions for the FEM element model,
 (a) The chosen boundary conditions for the FEM element model,
(a) The chosen boundary conditions for the FEM element model,
The chosen boundary conditions for the FEM element model,
he chosen boundary conditions for the FEM element model,
e chosen boundary conditions for the FEM element model,
 chosen boundary conditions for the FEM element model,
chosen boundary conditions for the FEM element model,
hosen boundary conditions for the FEM element model,
osen boundary conditions for the FEM element model,
sen boundary conditions for the FEM element model,
en boundary conditions for the FEM element model,
n boundary conditions for the FEM element model,
 boundary conditions for the FEM element model,
boundary conditions for the FEM element model,
oundary conditions for the FEM element model,
undary conditions for the FEM element model,
ndary conditions for the FEM element model,
dary conditions for the FEM element model,
ary conditions for the FEM element model,
ry conditions for the FEM element model,
y conditions for the FEM element model,
 conditions for the FEM element model,
onditions for the FEM element model,
nditions for the FEM element model,
ditions for the FEM element model,
itions for the FEM element model,
tions for the FEM element model,
ions for the FEM element model,
ons for the FEM element model,
ns for the FEM element model,
s for the FEM element model,
 for the FEM element model,
for the FEM element model,
or the FEM element model,
r the FEM element model,
 the FEM element model,
the FEM element model,

reinforcement and an initial crack (0 mm thick) from the hole to the boundary. The material outside the hole and the crack is modelled as isotropic and linear elastic with a Young's modulus of $E = 25 \times 10^9$ Pa and Poisson's ratio of 0.2. Furthermore, a uniform pressure applied normal to the cylindrical perimeter of the hole represents the pressure from the expansion caused by corrosion products. As a result of the symmetry, the FEM analysis is conducted on a quarter of the beam element considered.

4.2 Qualitative considerations of the shape changes of the crack

An important observation made under the numerical study of the crack opening was that, for different crack lengths, the influence of the remaining strength of the adjacent uncracked cross-sections was significant for the shape of the crack. The crack openings for four selected crack lengths are illustrated in figure 8.

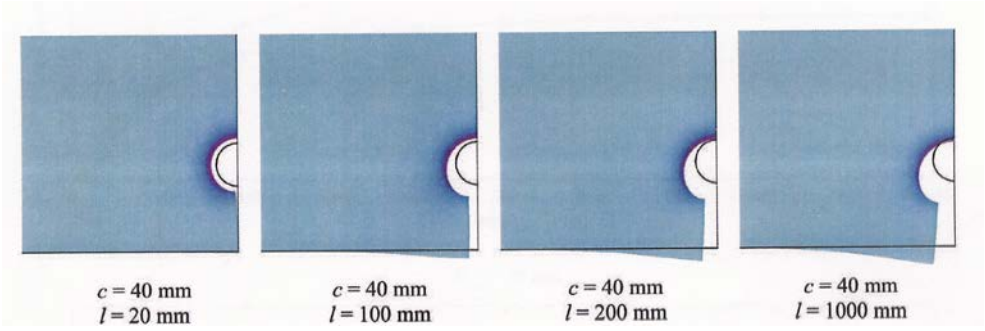

Figure 8. Illustration of the hole and the crack profile for 4 different lengths of the corroded part of the rebar. D_{bar}=20 mm.

The increases in crack openings at the surface Δw_{crack} and near the hole Δw_{hole} as a function of the crack length l are shown in figure 9. It can be noted that Δw_{crack} - Δw_{hole} is positive for l > 135, 90 and 60 mm for D_{bar} = 16, 20 and 25 mm, for a 40 mm cover respectively.

4.3 Estimation of the crack-corrosion index

In this section, the crack corrosion index is estimated from the shape changes of 3D FEM models with different bar diameters, covers, and crack lengths. The FEM analysis is performed with 5 covers c = 20, 30,…, 60 mm for 20 different crack lengths l = 10, 20,…, 100, 200,…, 1000 mm and for 3 different rebar diameters D_{bar} = 16, 20 and 25 mm. This is an extension of the investigation in Thoft-Christensen et al. (2005), which includes the variations of cover and crack length but with one rebar diameter on 20 mm. In figure 10, two different series of calculations of the crack corrosion index are shown. To the left the crack corrosion index based on the shape changes of the middle section and to the right based on an average of the cross sections shape changes in the entire crack. In figure 11, the data are represented with a 3D-plot and contour curves for easy reading of γ-values.

Note that the crack-corrosion index γ decreases with increasing values of the cover. The curves in figure 10 are obtained by a regression analysis, which is presented in the next section.

4.4 Estimation of the crack-corrosion index γ by curve fitting

A simple least-square regression analysis has been performed on the crack-corrosion index γ estimation shown in figure 10. The chosen regression formulas are

$$\gamma = \left(F_1^{\beta} \exp\left(F_2^{\beta} (1-l)^{F_3^{\beta}} \right) + F_4^{\beta} \right)(\alpha - 1) \tag{7}$$

$$F_i^{\beta} = f_{i1}^{\beta} + f_{i2}^{\beta} D + f_{i3}^{\beta} c + f_{i4}^{\beta} D^2 + f_{i5}^{\beta} Dc + f_{i6}^{\beta} c^2 \quad \text{for} \quad i \in \{1,2,3\} \quad \beta \in \{m,e\} \tag{8}$$

where β may be either *m* or *e* corresponding to the coefficient for γ calculated for the middle section or γ calculated as a average for all the sections in the entire crack. The components of f_{ij}^{β} is given in following matrices

$$\mathbf{f}^m = \begin{bmatrix} 2.22 & 1.43e2 & -8.79e1 & -2.13e3 & 2.03e2 & 5.57e2 \\ -2.25e-1 & -1.83e1 & -2.16e1 & 9.06e2 & -2.90e2 & 2.13e2 \\ 4.39e1 & 6.30e2 & -1.30e3 & -5.72e3 & -5.59e3 & 1.17e4 \\ 1.64e-1 & 2.80e1 & -6.32 & 2.23e2 & -1.59e2 & 9.87e1 \end{bmatrix} \tag{9}$$

$$\mathbf{f}^e = \begin{bmatrix} 2.25 & 1.24e2 & -8.89e1 & -1.46e3 & -1.00e2 & 6.44e2 \\ 1.76e-1 & -6.20e1 & -1.90e1 & 1.93e3 & -2.64e2 & 1.63e2 \\ 3.18e1 & 6.91e2 & -8.97e2 & -1.34e4 & -1.23e3 & 7.28e3 \\ 1.02e-2 & 9.07e1 & -1.10e1 & -1.88e3 & 5.03e2 & -3.37e1 \end{bmatrix} \tag{10}$$

The curves corresponding to (7) to (10) for α = 4.2 were shown in figure 10.

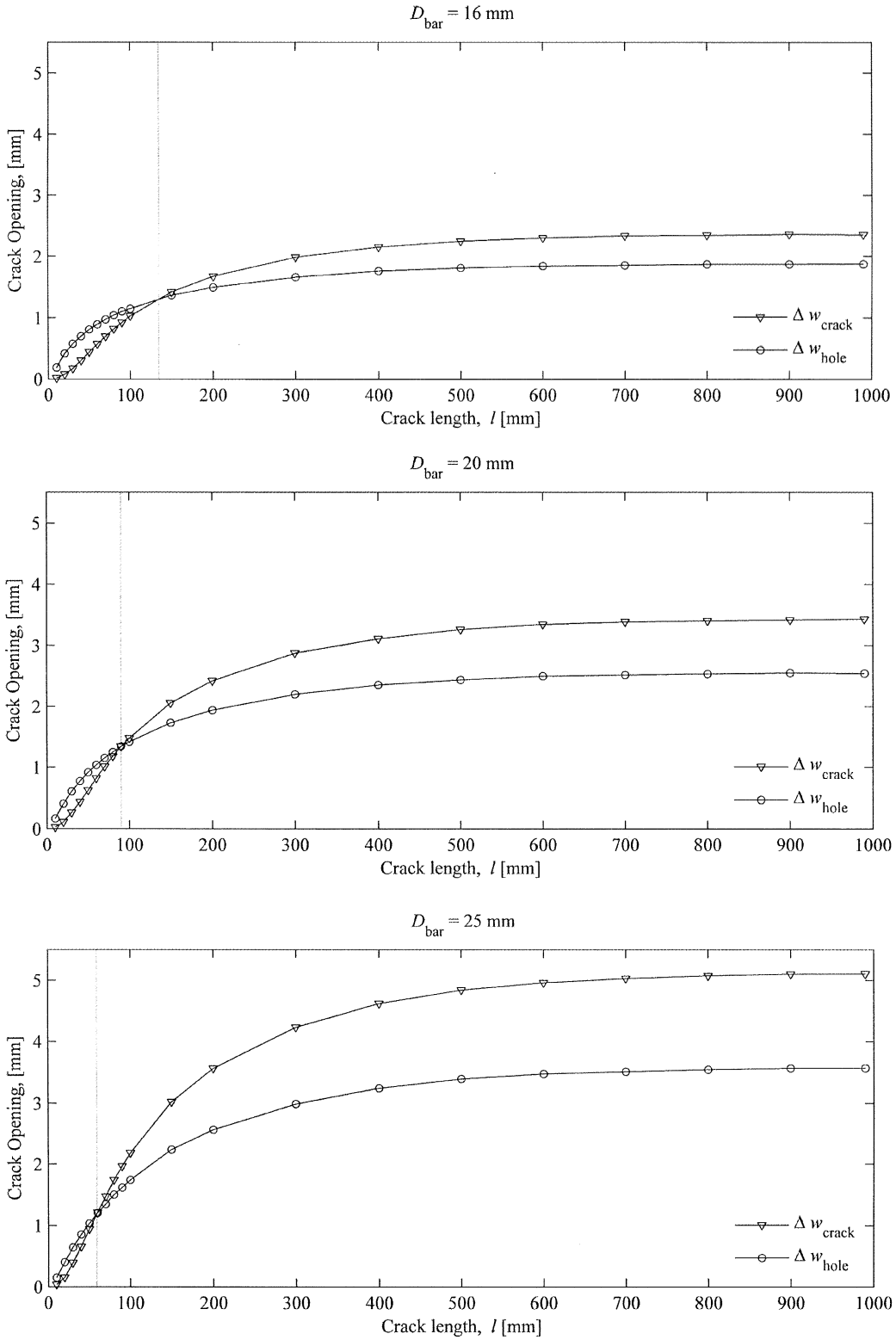

Figure 9. The crack openings for a beam with 40 mm cover at the surface Δw_{crack} and near the hole Δw_{hole} as a function of the crack length l.

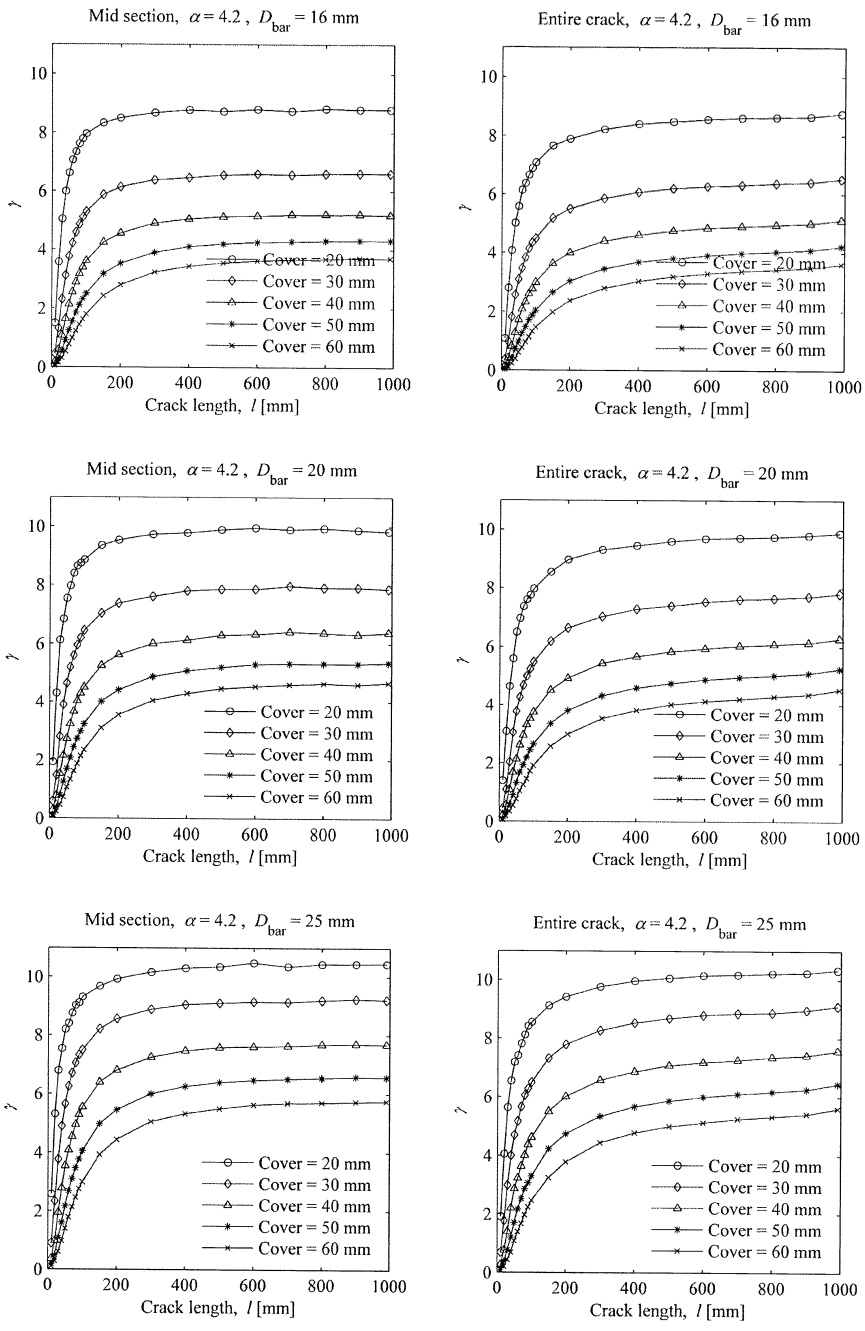

Figure 10. The crack-corrosion index γ as a function of the length of the corroded part of the rebar l, cover c and rebar diameter D_{bar} for the center cross section to the left and an average for the entire crack to the right. The symbols ○, ◊, Δ, * and × correspond to covers on 20, 30, 40, 50, and 60 mm, respectively. The curves are based on the regression analysis shown in section 4.4.

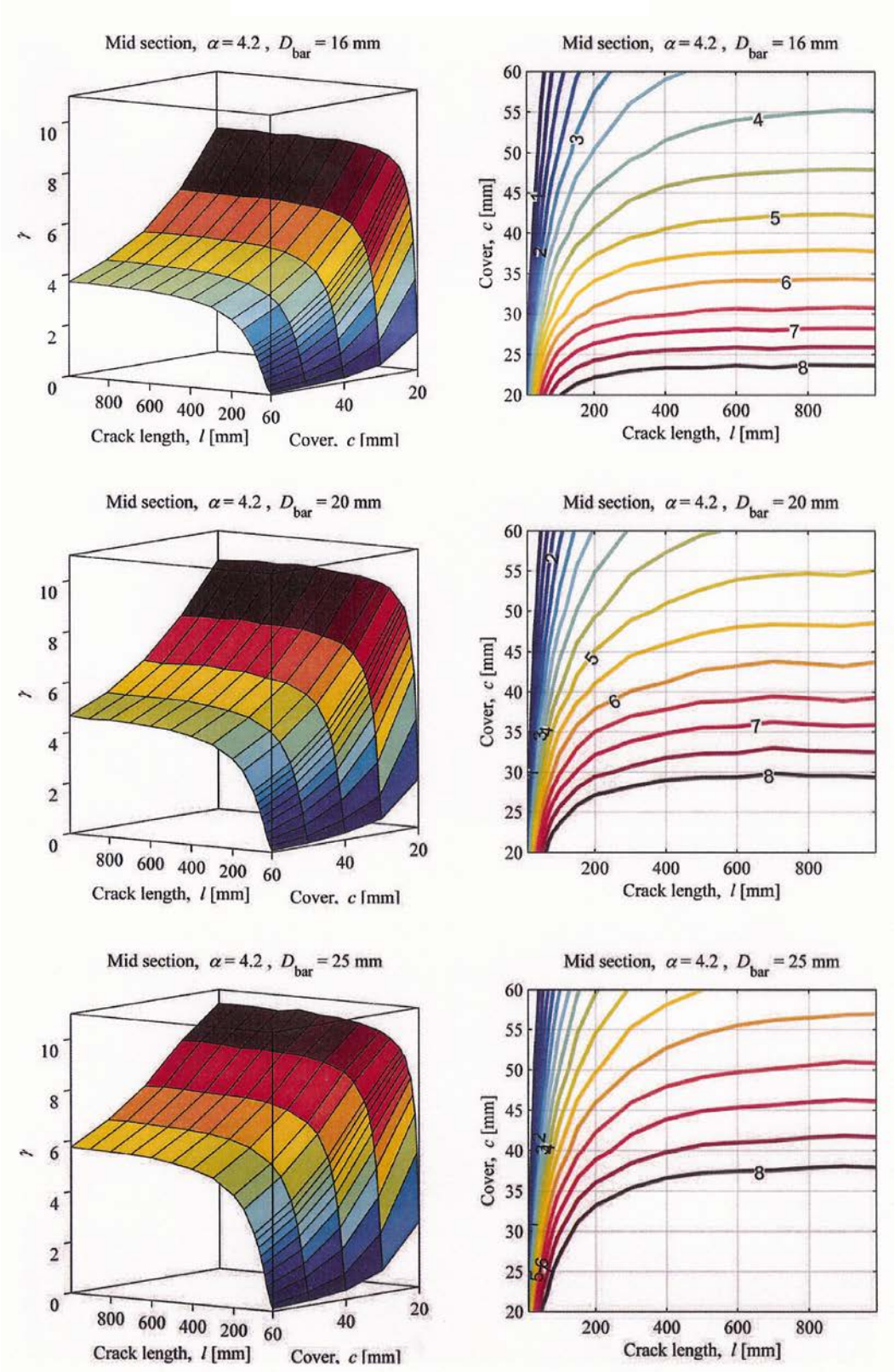

Figure 11. The crack-corrosion index γ as a function of the length of the corroded part of the rebar l, cover c and rebar diameter D_{bar} for the center cross section.

4.5 Pit Corrosion

In figure 12, the displacements are shown for the relatively short crack length l = 20 mm (pit corrosion), D_{bar} = 20 mm, and the cover is 40 mm. Note that the increase of the crack volume per length ΔA_{crack} (see figure 3) is small compared with cylindrical volume around the corroded part of the rebar.

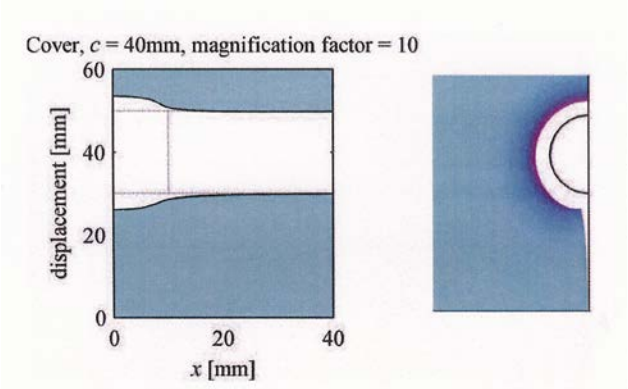

Figure 12. The displacement fields parallel and normal to the rebar for a short crack (pit corrosion).

The crack-corrosion index estimates shown in figure 10 indicate that the index γ varies moderately when the corrosion length l is greater than 300 mm of the length of the beam. However, for small values of l the index γ is reduced drastically. For very small values of l the index γ approaches zero. It can therefore be concluded that the approach used in this paper is not useful in the case of pit corrosion. This is as expected since the stiffness of the beam near the pit corrosion is very high as the pit corrosion crack is of little influence on the stiffness.

5. CONCLUSIONS

Models for the deterioration of reinforced concrete structures are presented with special emphasis on the corrosion crack opening during corrosion of the reinforcement. Experiments and 2-dimensional FEM analysis support that the relation between the reduction of the reinforcement diameter ΔD_{bar} and the corresponding increase in crack width Δw_{crack}, measured on the surface of the concrete specimen may be approximated by a linear function. In this paper, the crack-corrosion index has been extended to more realistic 3D-models of the cracked concrete beam. The crack corrosion index may then be evaluated for a 3-dimensional beam by assuming a concentrated corrosion area of the reinforcement.

It has been shown that by equalizing the volume of the produced rust products with the volume due to the expansion of the hole and the increased crack volume, the reductions of the rebar cross-sectional area and thereby the safety of the beam may be estimated. The results presented in this paper are preliminary outputs of an ongoing research.

For multiple cracks located along adjacent rebars, the method may be applied if the rebars are more than three times the diameter, since the stress field contributing to the deformations at this distance is negligible. For closer located rebars further investigations and research must be performed.

REFERENCES

[1] Thoft-Christensen, P., S. Svensson and H.L. Frandsen. 3-D Modelling of Corrosion Crack Opening. Proceedings of IFIP WG 7.5 Conference, Aalborg, Denmark, May 2005. In "Advances in Reliability and Optimization of Structural Systems" (eds. J.D. Sørensen and M. Frangopol), Taylor & Francis, 2006, pp.163-170.

[2] Thoft-Christensen, P., Estimation of the Service Lifetime for Concrete Bridges. In Proçeedings ASCE Structures Congress XV, Portland, Oregon, USA, 1997, pp. 248-252.

[3] Thoft-Christensen, P. Modelling of the Deterioration of Reinforced Concrete Structures. Proc. IFIP WG7.5 Conference on "Optimization and Reliability of Structural Systems", Ann Arbor, MI, USA, 2000, pp. 15-26.

[4] Liu, Y. & R.E. Weyers, Modelling of the Time to Corrosion Cracking in Chloride Contaminated Reinforced Concrete Structures. 1998. ACI Materials Journal, 95, 675-681.

[5] Du, Y.G., Chan, A.H.C. & L.A. Clark, Finite Element Analysis of the Effect of Radial Expansion of Corroded Reinforcement. Computer and Structures, Vol. 84, 2006, pp. 917-929.

[6] Bhargava, K., Ghosh, A.K., Mori, Y. & S. Ramanujam, Analytical Model for Time to Cover Cracking in RC structures due to Rebar Corrosion. Nuc. Eng. Des. Vol. 236, 2006, pp. 1123-1139.

[7] Thoft-Christensen, P. Assessment of the Reliability Profiles for Concrete bridges. Engineering Structures, Vol. 20, 1998, pp. 1004-1009.

[8] Thoft-Christensen, P. Stochastic Modelling of the Crack initiation Time for Reinforced Concrete Structures. Structures Congress, Philadelphia, USA, 2000.

[9] Andrade, C., Alonso, C. & F.J. Molina, Cover Cracking as a Function of Bar Corrosion: Part 1-Experimental Test. Materials and Structures, 1993, 26, 453-464.

[10] Nielsen, A, Hvid, grøn og sort rust (in Danish), Nordisk Beton, Vol. 2, 1976.

[11] Thoft-Christensen, P., Modelling Corrosion Cracks. Presented at the IFIP TC7 Conference, Sophia Antipolis, France, July 2003. In J. Cagnol and J-P. Zolesio (editors), Information Processing: Recent Mathematical Advances in Optimization and Control. Mathematical Computational Sciences, Presses de l'Ecole des Mines de Paris, 2004, pp. 25-33.

[12] Thoft-Christensen, P. FEM Modelling of the Evolution of Corrosion Cracks in Reinforced Concrete Structures. Proc. IFIP WG7.5 Conference on "Optimization and Reliability of Structural Systems", Banff, Canada, Nov. 2003, September 25-27 2003,pp. 221-228.

[13] Thoft-Christensen, P., Service Life Definitions Based on Corrosion Crack Width. Proceedings of the ICOSSAR 05, Rome, Italy, June 2005 (eds. G, Augusti, G.I. Schuëller, M. Ciampoli, CD, Millpress, 2005.